

# RESEARCH MEMORANDUM

PERFORMANCE OF A SUPERSONIC ROTOR HAVING HIGH MASS FLOW

By Ralph L. Schacht, Arthur W. Goldstein, and Harvey E. Neumann

Lewis Flight Propulsion Laboratory

# CLASSIFIED DOCUMENT This material contains information affecting the National Defense of the United States within the meaning the espionage laws, Title 18, U.S.C., Secs. 793 and 794, the transmission or revelation of which in are more to an unauthorized person is prohibited by law. ONAL ADVISORY COMMITTEE WASHINGTON July 19, 1 NATIONAL ADVISORY COMMITS

# NATIONAL ADVISORY COMMITTEE FOR AERONAUTICS

# RESEARCH MEMORANDUM

PERFORMANCE OF A SUPERSONIC ROTOR HAVING HIGH MASS FLOW

By Ralph L. Schacht, Arthur W. Goldstein, and Harvey E. Neumann

### SUMMARY

A 14-inch supersonic mixed-flow rotor with a supersonic leading edge and an inlet radius ratio of 0.52, designed for impulse operation and uniform work output, was tested in Freon-12. The highest efficiency was attained at 110 percent of design speed. At this speed the rotor developed a stagnation pressure ratio of 8.5 and an efficiency of 82.5 percent at a weight flow rate of 63.7 pounds per second (equivalent air value, 31.5 lb/sec/sq ft frontal area). At design speed (686 ft/sec in Freon-12 or 1480 ft/sec in air), these parameters had the values 5.3, 76.8 percent, and 63.2 pounds per second, respectively. With shock-inrotor operation, there was only a small range in weight flow with surge-free operation. An extremely high level of turbulence at the discharge indicated large regions of separated flow even for the impulse mode of operation. The efficiency of the rotor was very sensitive to either the inflow relative angle or the relative Mach number at the root or both.

Good agreement was obtained between the axisymmetric method of design and the measured pressure distribution on the casing except for two small regions where deviations are believed to have originated in the induction process, which is inadequately described by the assumption of axially symmetric flow. Casing pressure distribution varies with speed and guide vane settings, but these variations are not critical for this rotor in determining the over-all efficiency.

Friction with the casing was of negligible magnitude for this impeller. Losses other than casing friction indicated that the blades of this impeller were less efficient than the blades of the previously tested impeller.

### INTRODUCTION

The results are presented of an experimental study made at the NACA Lewis laboratory of a supersonic mixed-flow impeller of the shock-less type which had a "supersonic leading edge." (A supersonic leading edge is defined as one so oriented that the gas velocity component in the plane normal to that edge is supersonic.) This report is the third

describing an investigation of the aerodynamic problems involved in developing a supersonic compressor with shockless flow in the rotor at an isentropic pressure ratio of about 8.0 and nearly the maximum possible air flow per unit frontal area.

The 14-inch tip diameter and the inlet and exit conditions for the three rotors tested thus far were maintained the same in order to minimize test rig modification and to provide a simple variation for comparison of the rotors. The blades of all three rotors were of constant thickness (1/8 in.) in order to permit the use of welded sheet metal construction, but with the fabrication techniques developed it was possible to complete only rotor I (radius ratio 0.71) by welding. Rotors II and III were machined from solid billets. References 1 and 2 report on two rotors that were similar except that the weight flow was increased from 21.6 to 31.5 pounds of air per second per square foot frontal area by continuation of the blade surfaces inward along radial lines to the modified hub, which was located on the streamline intersecting the leading edge at a radius ratio of 0.52 instead of the value 0.71 used in the first rotor. These rotors had subsonic leading edges, that is, the leading edges were swept back for subsonic normal gas velocities.

It was expected that some effect of this edge on starting of the internal supersonic flow (swallowing the strong induction shock) might be detected from a comparison of the characteristics of the rotor having a supersonic leading edge with the two having subsonic leading edges. Other characteristics as well as the effect on the inlet flow and range of efficient operation were also examined during this exploratory project.

# EQUIPMENT AND PROCEDURE

# Rotor Design

The rotor design is for 22 blades of constant thickness (1/8 in.) to operate at an isentropic pressure ratio of about 8.0, an equivalent tip speed of 1480 feet per second (686 ft/sec in Freon-12), and an inlet axial Mach number of about 0.85. The inflow has zero radial velocity and rotates as a free vortex counter to the wheel rotation. The internal flow is shockless. Relative discharge flow is nearly axial. Inlet and outlet velocity diagrams for root and tip sections are shown in figure 1.

The leading edges are swept back in a manner determined by the inlet flow, the prescribed blade shape at the root, and the condition of radial blade elements. The result of these assumptions was a leading edge operating with a supersonic gas velocity component in the plane normal to the leading edge. The leading edges were oriented so that the initial suction surface paralleled the expected upstream flow, and a 10° wedge for the initial blade thickness distribution determined the pressure surface (see table I). At or downstream of a point where an expansion wave originating on the suction surface would intersect the leading edge of the next blade, a suction surface deflection (expansion) of 10° was begun and was completed at the channel entry in such a manner that the full thickness of 1/8 inch was attained at that point. This provided an eventual cancellation of the original 10° wedge shock and enlarged the flow area inside the blades as compared with the flow area upstream. Inside the channel the method described in references 1 and 3 was used to complete the design.

Because the gas was turned toward the axial direction by blades of constant thickness, the flow area and Mach number increased inside the channels. In the first two rotors with swept leading edges it was possible to counteract this effect by means of compression waves originating from the hub. With the present impeller, however, the first hub wave strikes the casing at a point well inside the impeller (see fig. 2). It is therefore impossible to prevent this velocity rise upstream of that point with cambered constant thickness blades.

The mean channel relative velocity at the tip increased from a value of 952.2 feet per second to 1135.6 feet per second in this initial region. This mean channel velocity was then decreased at the rate of 1 percent per length equal to one momentum thickness (ref. 4) until the initial inlet value was again reached at the exit. As a consequence of the rise of the channel velocity in the initial portion of the rotor, very little work was done on the gas in this region, and the rotor obtained was longer than that with the subsonic leading edge.

The assumption of constant work output and zero radial velocity component for the exit flow then determined a free-vortex flow at the exit. Work output was equalized by sweeping the trailing edges back to provide extra blade surface at the root for work input.

The hub shape was then determined according to the method of reference 3. The complete characteristic network and Mach contours are shown in figure 2.

These design computations resulted in a very smooth velocity distribution on the hub, but the tip velocity distribution was characterterized by a large expansion followed by a compression. Because the hub velocity distribution was much smoother than that of the swept impeller, testing the present rotor would provide an opportunity to find whether the efficiency was more sensitive to velocity variations at the hub or casing.

The growth in displacement thickness of the boundary layer was assumed to be 0.02 inch per inch of gas travel on the wetted surfaces. The correction for all the surfaces was made on the hub.

The coordinates of the blade surface and the hub contour which resulted from this design procedure are given in table I. A photograph of the rotor is shown in figure 3.

# Test Rig, Instrumentation, and Procedure

The test rig installation was the same as described in reference 1 and is shown in figure 4. The working fluid was Freon-12 which was circulated in the closed system diagrammed in figure 5.

Inlet stagnation temperatures and pressures were measured in the surge tank and four static-pressure taps in the nozzle were used for determining the weight flow after calibration with numerous surveys at station 1. At station 1, three claw probes were used with four static-pressure taps on the hub and four on the casing.

Measurements of the discharge flow were made at station 4 with three semishielded thermocouple probes and three pressure probes; for pressure measurements with shock-in-rotor operation, claw probes were used; and for impulse operation of the rotor, when a very high Mach number was encountered, the wedge probes were used. Hot-wire anemometers were also used at three circumferential locations at stations 1 and 4 to study the nonsteady flow qualitatively. The steady-flow instruments were the same as those used to obtain the data reported in reference 2, with the exception that the span of the wedge probe was increased from 0.3 to 0.4 inch to ensure freedom from end effects on the wedge readings.

Even though the instrumentation and inlet flow conditions were nearly identical with those of the tests reported in reference 2, there are some discrepancies in the checks. For impulse operation, calculation of the weight flow from the exit survey gave a value of 59.6 pounds per second, whereas the value from the nozzle calibration was 62.2 pounds per second - an error of -4 percent. For the previous tests the error was only +1 percent. For the present tests the equivalent specific enthalpy rise as determined from the thermocouples was only 1 percent lower than that found from the corrected dynamometer power and nozzle determined weight flow, whereas with the data of reference 2 a discrepancy of +6.5 percent was found. There is a possibility that the different behavior of the instruments results from nonsteady flow conditions which vary from one impeller to another, but which are not detectable by the instruments. This is indicated by the different regions of rotor audible surge which will be described in more detail in the next section.

The performance of this impulse-type supersonic compressor was determined over a range of back pressures from open throttle to audible surge at seven wheel speeds from 110 percent of the design value to 50 percent of the design value. The inlet tank pressure was maintained at 15 inches mercury absolute during all tests, and inlet stagnation temperature varied from  $60^{\circ}$  to  $140^{\circ}$  F, depending on the load on the cooling system. Freon purity was maintained over 97 percent at all times. The impulse points were run twice, once with the guide vanes set the same as with the previous impeller with a subsonic leading edge and once with the guide vanes reset for  $8^{\circ}$  more counterrotation.

# RESULTS AND DISCUSSION

# Over-All Rotor Performance

The rotor was found to operate in a manner similar to the two previous rotors with subsonic leading edges (refs. 1 and 2), that is, with two modes of operation. In the first mode a system of shocks was located in the rotor near the entrance and caused a relative Mach number of approximately 1.0 inside and a relative subsonic velocity at the exit. As the throttle was opened the weight flow increased to a limit and further opening caused the internal shock to pass from the leading edge through the rotor, so that the relative internal velocities became supersonic. With the discontinuous change in mode from shock-in-rotor to impulse operation, the weight flow remained practically unchanged; but the pressure ratio, the efficiency, and the equivalent specific stagnation enthalpy rise  $\Delta H_{\rm e}$  of the gas all changed discontinuously to higher values. (A list of symbols is given as an appendix.)

The two rotors with subsonic leading edges went over to impulse operation at 60 and 68 percent of design speed, respectively, while the present rotor would not operate in the impulse mode until 80 percent of design speed.

At all speeds where impulse operation was possible, practically no range of gas flow was obtained before encountering audible surge. This was not true for the impellers with subsonic leading edges (impellers I and II), where there was a range of about 14 percent in gas flow before encountering audible surge. It was possible to operate impeller III in surge through the same range of weight flows as the previous 0.52 inlet radius ratio impeller (impeller II) without any violent surge or mechanical failure.

Hot-wire anemometers used to check this surging condition confirmed the fact that the impeller had a very small weight flow range with stable operation. During surge at design speed, the hot wires at station 1 showed the weight flow to oscillate with a frequency of 10 to 15 cycles per second with the root and tip fluctuations 180° out of phase. At station 4 the root and tip variations were in phase. All these changes took place simultaneously around the entire annulus. For impulse operation at design speed, the hot wires at station 4 showed a very high level of turbulence (flow varied from 50 to 150 percent of average value) and the blade wakes were not identifiable.

At 80 percent of design speed similar surge variations were obtained; only a slight reduction in turbulence level was obtained at impulse operation. Such a high turbulence level indicates probable flow separation inside the rotor.

The over-all performance of the rotor in terms of equivalent weight flow  $W_e$ , equivalent rise in specific stagnation enthalpy  $\Delta H_e$ , pressure ratio, and efficiency for various speeds is shown in figure 6. (The operating points on all figs. in this report are indicated by numbers which designate the ratio of speed to design speed and the letter I or S, which indicates either impulse or shock-in-rotor condition.) The maximum efficiency of 82.5 percent occurred at 110 percent of design speed where a pressure ratio of 8.5 was developed with a flow of 63.7 pounds of Freon per second. Comparison of the performance of rotors II and III results in the following notes:

- 1. At 60, 70, and 80 percent of design speed, the weight flows passed by impeller III are greater than those passed by impeller II. The weight flows passed at 90 and 100 percent of design speed are the same for both impellers and are very close to the design value.
- 2. At 80 percent of design speed impeller III imparted to the gas the same rise in stagnation enthalpy with shock-in-rotor operation as impeller II, but imparted less of an increase of  $\Delta H_{\rm e}$  in passing to impulse operation. At 90 and 100 percent of design speed the work input to the gas was lower at all conditions of operation and the increase in work input in passing from shock-in-rotor to impulse operation was less than that of rotor II. Although this difference between the rotors is not to be expected from the blade shape, since the trailing edge surfaces and the loading in the rear of the blades were the same for both rotors, there is about 5 percent difference in the moment of momentum increment of the gas. This is only about one-third of the difference in enthalpy rise and therefore the decrease in work input is a result of lower friction with the casing.
- 3. The efficiencies for rotor II at impulse operation are all higher than those for rotor III except at the design speed, where the two impellers have the same efficiency.

# 320

# Entrance Flow

At design speed, the entrance relative Mach numbers are only 0.05 lower than the design values (fig. 7(a)). However, the values are 0.1 lower than those obtained with impeller II. This indicates an upstream effect of the rotor which depends on the sweep and the shape of the leading edges of the rotor blades. This effect on the upstream flow is also apparent in the comparison of the absolute Mach numbers (fig. 7(b)), where a lower value is also shown for impeller III. The same set of inlet guide vanes was used for both rotors.

Relative inflow angles (fig. 7(c)) are about  $2.5^{\circ}$  higher than for the swept rotor, again indicating an upstream effect for the rotor which depends on the sweep. When the guide vanes were reset for  $8^{\circ}$  more counterrotation (fig. 7(d)), the weight flow was reduced because of choking of the guide vanes. The relative inlet angles were not affected near the pitch section, although the change at the hub was  $+1.5^{\circ}$  and at the tip was  $-1.5^{\circ}$ . This behavior is similar to that of the two rotors with swept blades, where the relative inflow directions were also determined by the rotor. In fact, with the 0.71 inlet radius ratio rotor two sets of guide vanes were used that gave an absolute angle change of  $6.5^{\circ}$ ; yet the relative angles showed a maximum variation of only  $0.5^{\circ}$ .

The angle of attack on the suction surface of the blade varies from  $6^{\rm O}$  at the root to  $4^{\rm O}$  at the tip and indicates the inadequacy of the two-dimensional cascade analysis, which predicts that for subsonic axial velocities the direction of inflow for a supersonic flow is set by the direction of the suction surface of the blades at the leading edge. This  $5^{\rm O}$  discrepancy may be a consequence of the slight sweep of the blades, which varies from about  $18^{\rm O}$  (complement of angle between flow vector and leading edge) at the tip to about  $48^{\rm O}$  at the root, or may result from the root-to-tip pressure balance requirements which also alter the flow from that expected from a two-dimensional flow.

If the relative flow angles and Mach numbers are compared with the blade direction, it is apparent that at least a portion of the pressure surface of the blade must suffer a detached shock for most conditions of operation. At 70 percent of design speed, this condition exists over the entire leading edge; at 80 percent of full speed approximately 50 percent of the blade span requires detached shock; while at design speed this condition exists for only a small region near the root. When the inlet guide vanes were reset, substantially higher Mach numbers were obtained with approximately the same relative flow direction with respect to the rotor blades. Consequently the deflection for induction into the rotor did not imply a detached shock for any of the speeds investigated. The increase in efficiency at equal speeds was greatest at the lowest speed (8 percent increase in  $\eta_{\rm ad}$  at 80 percent speed), where

the greatest reduction in extent of span suffering detached shock

occurred. At design speed there was only a small increase in efficiency. This indicates that the amount of inlet area sustaining detached shock possibly is a critical factor in establishing the variation of efficiency. The inlet area and other conditions, such as Mach number and the resulting internal pressure distribution, change simultaneously; consequently the variation of efficiency cannot be definitely ascribed to this one factor.

# Distribution of Static Pressure on Casing

In the design process the pressure distribution along the casing as shown by figure 8 was computed. The data for this impeller at design speed are also shown on this figure. Fairly good agreement is shown between the axisymmetric method of design and the experimental results except near the leading edge (z = approximately 3.0 in.), where the pressure is much higher than the design value, and in the region near z = 7 inches, where the pressure is too low. The assumption of axial symmetry of the flow is believed to approximate the flow because of the satisfactory estimates of pressure distribution it gave over most of the casing. The local deviations from the estimates at z = 3inches and z = 7 inches are therefore thought to result from pressure waves originating in regions where the assumption does not approximate the actual flow. This would include regions where the blades are highly loaded and also the inlet section of the blades where the flow is not yet enclosed and guided by channels as the theory assumes to be the case. Inasmuch as the blade loading is very light, the deviations are ascribed to the inadequacy of the axisymmetric assumption for estimating the inflow process.

Figure 8 shows the pressure distribution along the casing for impulse operation at several speeds with the original and reset guide vanes. The measured and calculated pressure rise in the neighborhood of z=4.5 inches is caused by the hub deflection beginning at z=0, as can be seen by tracing the characteristic lines. At lower gas velocities there is an expected forward shift of the pressure wave.

For the purpose of correlating the internal losses with other factors, the loss, which is calculated from

Loss = 
$$\Delta H_e(1 - \eta_{ad})$$

is made dimensionless through division by the averaged inlet relative kinetic energy per unit mass. Three parameters are noted for comparison with the loss - the rotative speed, the maximum relative internal Mach number as indicated by the casing pressure taps, and the maximum rate of local pressure rise as determined from the casing pressure taps.

To illustrate the calculation of the rate of pressure rise, at 80 percent of full speed for the original guide vanes the major portion of the rise occurs between z=4 inches and z=6.75 inches. The static-pressure ratio is 2.45. Approximating the relative stagnation pressure by the value at the inlet, there is obtained a value for  $(1/q)(\Delta P/\Delta z)$  of 0.256. Tabulation of the corresponding data with efficiency and the dimensionless values of the losses for other conditions yields:

Parameter	Guide vanes			
	Original		Reset	
	Percent of design spe			speed
	80	100	80	100
Adiabatic efficiency	0.72	0.77	0.80	0.79
$\frac{1}{q} \frac{\Delta P}{\Delta z}$ (1/in.)	.256	.123	.121	.127
Maximum tip Mach number Mass average loss/ average inlet kinetic energy	2.0	2.3	2.3	2.6

where

- q dynamic pressure  $(1/2 \rho V^2)$
- ΔP increase in static pressure
- $\Delta z$  change in distance parallel to axis of rotor

At each speed the loss is reduced by using the reset guide vanes. A reduction of loss is obtained at 80 percent of design speed with reduction of the diffusion factor  $(1/q)(\Delta P/\Delta z)$ , but the reduction of loss at 100 percent speed does not correlate with a corresponding reduction of diffusion factor. Furthermore, the pressure distributions, diffusion factors, and Mach numbers are very nearly equal for operation at design speed with the original guide vane settings and at 80 percent of design speed with reset guide vanes, yet there is a large difference in the losses. It may therefore be concluded that the casing pressure distribution is not a critical factor for this rotor in determining the efficiency. However, the highest efficiencies were approximately 80 percent for this rotor, so that the casing pressure distribution could prove to be important for a rotor of higher efficiency.

# Exit Flow

The loss distribution at the exit is shown in figure 9(a). The greatest losses are evident in the gas discharged near the tip. These losses did not necessarily occur at the tip, as any low-energy gas which clings to the blades would probably be centrifuged to the tip. It is of interest that when the guide vanes were reset, the losses remained the same at the tip, decreased in the center of the passage, and increased at the hub. This is true for all impulse points except at 80 percent of design speed, where the losses were reduced over the entire passage when the guide vanes were reset.

Actually, the two operating states most nearly comparable are design speed with the original setting of the guide vanes and 80 percent of design speed with reset inlet guide vanes, because at these conditions the inlet relative Mach numbers are nearly equal and the casing pressure distributions are nearly the same. The 80 percent speed point shows lower losses over the entire blade span at the exit. The only apparent differences between the two operating states are the rotative speed and slight variations of inflow angles (3.5°) near the tip and of relative inflow velocities near the root. It must therefore be concluded that the losses in this impeller are very sensitive to inflow angles or that the inlet Mach number is critical when it approaches the value which implies detached shock from the leading edge. This latter criterion appears plausible in view of an expected thick boundary layer near the root at the entrance. The losses are also shown by the adiabatic efficiency distribution in figure 9(b).

Friction with the casing caused considerable loss in the two previously tested impellers although there was an uncertainty as to the amount. For impeller III casing friction was negligible. The distribution of axial Mach number at the exit (fig. 9(c)) indicates a thicker boundary layer at the casing for impeller III than for impeller II and implies a difference in the flow and casing friction phenomena between the two rotors.

In reference 2 the losses exclusive of casing friction were divided by the specific work inputs and found to give a function that was constant with speed, indicating that if casing friction were negligible, the swept rotor might be expected to have an approximately constant efficiency of 87 percent for impulse operation at all speeds. Because casing friction is negligible for impeller III, the comparable figure is the adiabatic efficiency which attains a maximum over-all value of only 82.5 percent at 110 percent of design speed. Thus the blades of rotor II appear to be more efficient and less sensitive to inflow conditions but in some manner give rise to high values of casing friction. With a different thickness distribution for blades of little sweep, as in rotor III, an internal pressure distribution may be made similar to

that of rotor II with a possible increase in efficiency. The pressure distribution on the hub does not appear to have as decisive an effect on efficiency.

The relative discharge angles (fig. 9(d)) are very close to the design value for this impeller, whereas the two previous impellers indicated an unexplained overturning of about 4° in the center of the blade span. The blades were designed for a uniform specific work input to the gas from root to tip. The design value was 19.9 Btu per pound; the measured average value for this impeller was 20.3 Btu per pound with only a small variation from root to tip. The work equalizing property of the blades was therefore considered satisfactory as it was for the two previous impellers. The discharge Mach numbers and directions shown on figures 9(e) and (f) indicate that the diffuser has the difficult problem of handling effectively a large range of Mach numbers and inflow angles.

# SUMMARY OF RESULTS AND CONCLUSIONS

A 14-inch supersonic mixed-flow rotor with a supersonic leading edge and an inlet radius ratio of 0.52, designed for impulse operation and uniform work output, was tested in Freon-12. The highest efficiency occurred at 110 percent of design speed (686 ft/sec in Freon-12 or 1480 ft/sec in air). At this speed the rotor developed a stagnation pressure ratio of 8.5 and an efficiency of 82.5 percent at a weight flow rate of 63.7 pounds per second. Equivalent value for air is 31.5 pounds per second per square foot frontal area.

At the design point the rotor developed a pressure ratio of 5.3 and an efficiency of 76.8 percent at a weight flow rate of 63.2 pounds per second, whereas the estimated value was 64.7 pounds per second. The estimated value of work input was 19.9 Btu per pound and the measured value, 20.3 Btu per pound. Variation of enthalpy rise across the passage was small so that the work equalizing property of the rear portion of the blades was considered satisfactory.

At 80 percent of design speed the adiabatic efficiency was increased from 72 to 80 percent by 8° more counterrotation in the guide vanes. The existence of a steady detached shock in front of the blades with the original guide vane setting was probably involved in reducing the efficiency from the value obtained with the reset guide vanes. The magnitude of this change in efficiency cannot be explained by the change in shock losses, but is possibly affected by some interaction of the main flow and the boundary layer flow. At 100 percent speed where the relative inflow velocity was substantially over the critical value, resetting the guide vanes resulted in only a small change in efficiency.

Agreement shown between the axisymmetric method of design and the measured pressure distribution on the casing is considered adequate except for two small regions where deviations are believed to have originated in the induction process, which is inadequately described by the assumption of axially symmetric flow. Casing pressure distribution varies with speed and guide vane settings, but these variations are not critical for this rotor in determining the over-all efficiency.

Friction with the casing was of negligible magnitude with this impeller, while with the previous two impellers it caused considerable loss.

Losses other than those due to casing friction indicated that the unswept blades with the loading and pressure distribution concomitant with constant blade thickness were less efficient and more sensitive to variations in the inlet flow conditions.

The unswept blades of rotor III (present investigation) provided a negligible range of surge-free operation at all speeds where impulse operation was possible, whereas the swept blades of rotor II (ref. 2) provided at least a 14 percent range in weight flow. An extremely high level of turbulence at the discharge indicated large regions of separated flow even for the impulse modes of operation.

Lewis Flight Propulsion Laboratory
National Advisory Committee for Aeronautics
Cleveland, Ohio, April 23, 1954

# APPENDIX - SYMBOLS

The following symbols are used in this report:

- AH increase in specific stagnation enthalpy from station 0 to station 4, Btu/lb
- $\Delta H_{\rm is}$  increase in specific enthalpy at constant entropy from conditions at station O to  $P_{\rm T.4},$  Btu/lb
- M absolute Mach number, ratio of absolute velocity of fluid to local velocity of sound
- M' relative Mach number, ratio of velocity of fluid relative to rotor to local velocity of sound
- MA axial Mach number, ratio of axial component of velocity of fluid to local velocity of sound
- P static pressure, lb/sq in.
- $P_{\text{TP}}$  absolute stagnation pressure, lb/sq in.
- q dynamic pressure  $(1/2 \rho V^2)$
- r radial distance from axis of rotation, in.
- W mass flow of gas, lb/sec
- z distance parallel to axis of rotor, in.
- angle between axis of rotation and relative velocity vector, deg
- angle between axis of rotation and absolute velocity vector, deg
- $\eta_{ad}$  adiabatic efficiency of rotor,  $\eta_{ad} = \frac{\Delta H_{is}}{\Delta H}$

# Subscripts:

- o entrance tank upstream of nozzle (see fig. 5)
- 1 station 1 at rotor entrance (see fig. 4)
- station 4, 8 in. downstream of impeller blade tip (see fig. 4)
- e equivalent value for standard pressure and temperature

# REFERENCES

- 1. Goldstein, Arthur W., and Schacht, Ralph L.: Performance of a Swept Leading Edge Rotor of the Supersonic Type with Mixed Flow. NACA RM E52KO3, 1953.
- 2. Goldstein, Arthur W., and Schacht, Ralph L.: Performance of a Supersonic Mixed-Flow Rotor with a Swept Leading Edge and 0.52 Inlet Radius Ratio. NACA RM E53H27, 1953.
- 3. Goldstein, Arthur W.: Axisymmetric Supersonic Flow in Rotating Impellers. NACA Rep. 1083, 1952. (Supersedes NACA TN 2388.)
- 4. Goldstein, Arthur W., and Mager, Artur: Attainable Circulation about Airfoils in Cascade. NACA Rep. 953, 1950. (Supersedes NACA TN 1941.)

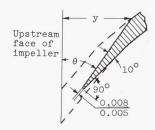
TABLE I. - COORDINATES OF BLADE MEDIAN SURFACE AND REGION NEAR LEADING EDGE<sup>a</sup>
[The symbols h and t are used to indicate hub and tip radii, respectively.]

Axial distance, z, in.	Radius, r, in.	Angular coordinate	Axial distance, z, in.	Radius, r, in.	Angular coordinate	Axial distance, z, in.	Radius, r, in.	Angular coordinate
0.0	b3.649	0	7.7	4.998h	640 4.41	11.0	b <sub>5.188</sub>	64°33.8'
0.5	3.656h	8 <sup>0</sup> 39.31		7.000t	640 4.41		5.206h	
	4.190t	8°39.3'	8.0	5.056h	64°33.2'		5.614	64041.2
1.00	3.680h	16°30.4'		5.049	64°33.2'		6.216	65° 1.5'
	5.503t	16°30.4'		5.614	64033.21		6.330t	
1.284	3.707h	20°36.5'		6.216	64°33.2'		7.000	67°25.8'
	7.000t	20 <sup>0</sup> 36.5'		7.000t	64031.51	11.5	b <sub>5.188</sub>	63046.41
1.5	3.733h	23 <sup>0</sup> 33.7¹	8.5	5.139h	65° 0.5'		5.200h	
	7.000t	23°33.7'		5.145	65° 0.5'		5.614	63055.81
2.0	3.812h	29049.81		5.614	65° 0.5'		6.070t	
	7.000t	29049.81		6.216	65° 0.5'		b6.216	64 <sup>0</sup> 44.1'
2.5	3.912h	35°16.4'		7.000t	65° 8.4'		b7.000	68 <sup>0</sup> 1.2'
	7.000t	35°16.4'	9.0	b5.188	65 <sup>0</sup> 28.1'	12.0	b5.188	62042.91
3.0	4.021h	39°57.5'		5.196h	65 <sup>0</sup> 28.1'		5.194h	
0.0	7.000t	39°57.5'		5.614	65°28.1'		5.614	62°58.91
3.5	4.130h	43056.21		6.216	65 <sup>0</sup> 28.1'		5.812t	
0.0	7.000t	43°56.21		7.000t	65°39.0'		b6.216	64°24.6'
4.0	4.245h	47031.01	9.5	b5.188	65°33.8'	9.82	b7.000	68 <sup>0</sup> 30.0'
1.0	7.000t	47°31.0'	""	5.219h	65°33.8'	12.5	b5.188	61°17.0'
4.5	4.356h	50049.11		5.614	65°33.81		5.190h	
4.0	7.000t	50°49.1'		6.216	65°34.0'		5.554t	
5.0	4.461h	540 4.61		7.000t	660 6.4'		b5.614	61059.01
3.0	7.000t	540 4.61	10.0	b5.188	65°30.1'		b6.216	64° 6.0'
5.5	4.566h	56°56.01	10.0	5.212h	65°30.1'		b7:000	68°58.81
5.5	7.000t	56°56.0'		5.614	65°30.1'	13.0	5.188h	59°36.91
6.0	4.666h	59°22.3'		6.216	65°31.5'	10.0	5.295t	
0.0	7.000t	59022.31		6.848t	00 01.0		b5.614	60°56.41
6.5	4.768h	61014.3'	1	b7.000t	66 <sup>0</sup> 32.0'		b6.216	63°45.6'
0.0	7.000t	61014.3	10.5	b5.188	650 9.21	4	b7.000	69°27.6'
7.0	4.867h	62042.41	10.5	5.208h	00 0.2	13.5	b5.188	57°48.0'
1.0	7.000t	62042.41		5.614	650 9.81	10.0	0.100	- 10.0
7 5		63043.81		6.216	65°17.9'			
7.5	4.961h	63043.81		6.589t	00 11.0			
	7.000t	65-45.8			670 3.01		17	
				b7.000	6/- 3.0.			

Coordinates for leading edge of blade

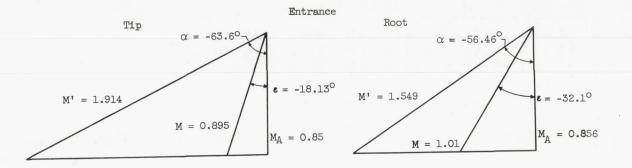
r	Z	У	θ	
7.000	1.284	1.426	26 <sup>0</sup> 24.0'	
6.500	1.204	1.451	27°39.6	
6.000	1.119	1.431	28048.2	
5.500	0.998	1.349	28°54.8	
5.000	0.852	1.223	30°54.0	
4.500	0.656	1.038	31054.6	
4.000	0.387	.773	32°52.2	
3.500	0.0	.387	33°48.6	

Typical section near leading edge of blades. Plane perpendicular to radius  $\, \, r \, \,$  at  $\, \, R \, . \,$ 



a\_The blade root begins at z=0.124 in., becomes nonradial at z=10.670 in., and ends at z=13.207 in. The section at r=5.614 in. begins at z=1.030 in., becomes nonradial at z=9.985 in., and ends at z=12.376 in. The section at r=6.216 in. begins at z=1.157 in., becomes nonradial at z=8.988 in., and ends at z=11.212 in. The tip begins at z=1.284 in., becomes nonradial at z=7.700 in., and ends at z=9.706 in.

bpoints used for blade layout only.



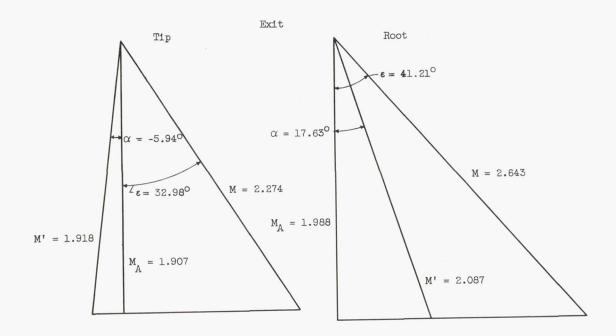


Figure 1. - Velocity diagrams at design for 14-inch supersonic compressor rotor.

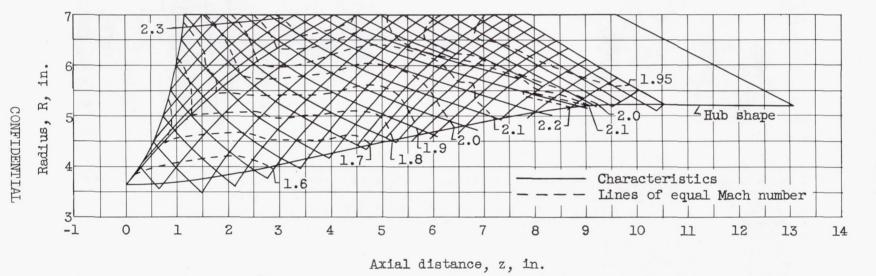
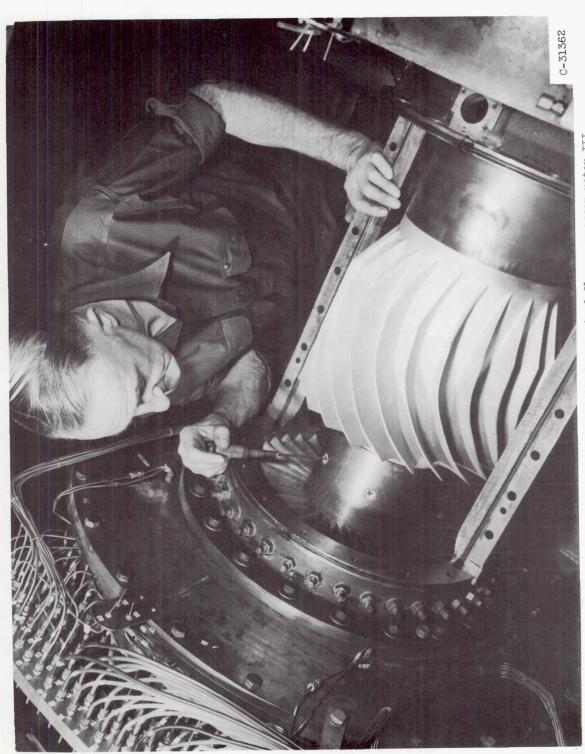


Figure 2. - Characteristic lines and velocity contours in rotor.



- 14-Inch supersonic axial-discharge mixed-flow compressor rotor III. 3 Figure

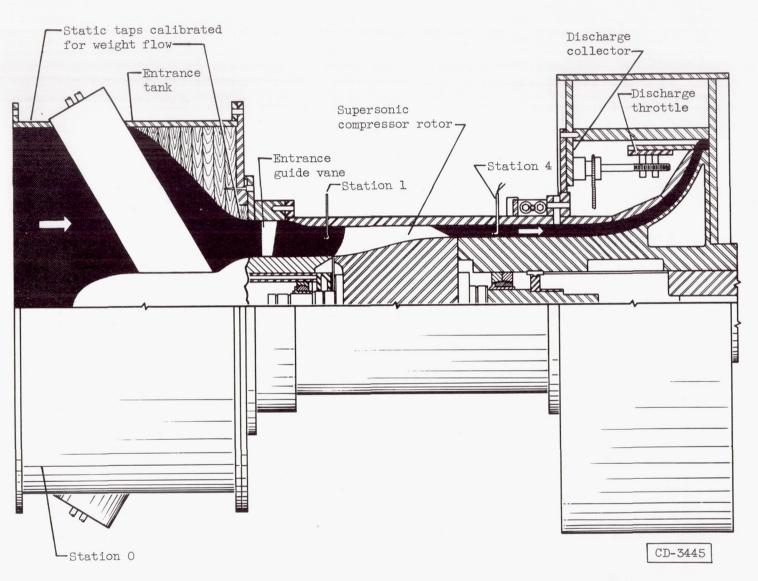
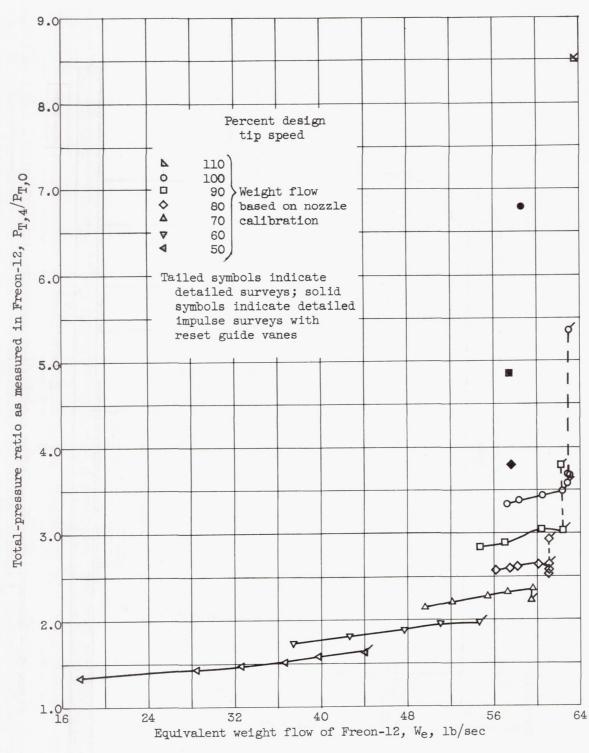


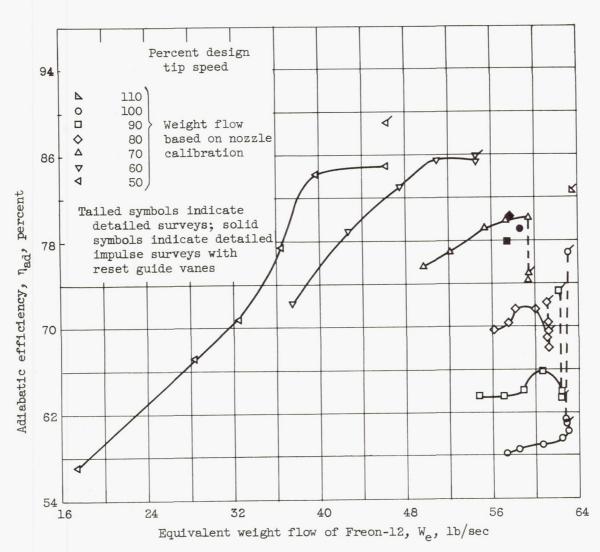
Figure 4. - Schematic diagram of 14-inch supersonic-compressor test rig.

Figure 5. - Schematic diagram of piping assembly and compressor installation.



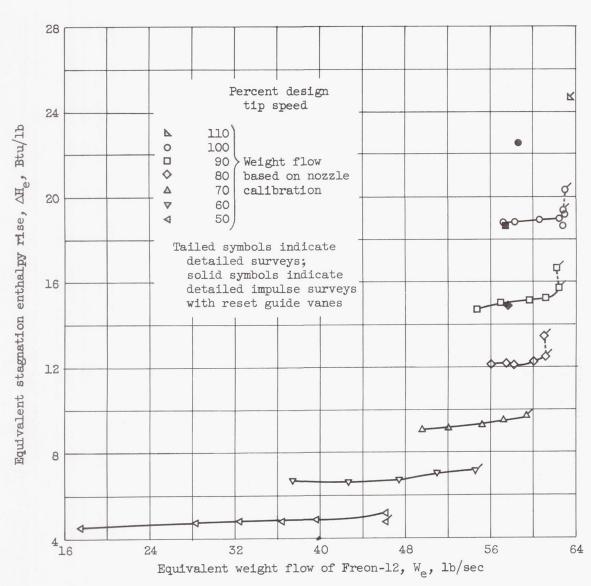
(a) Total-pressure ratio.

Figure 6. - Performance characteristics for 14-inch supersonic compressor rotor with supersonic leading edge.



(b) Adiabatic efficiency.

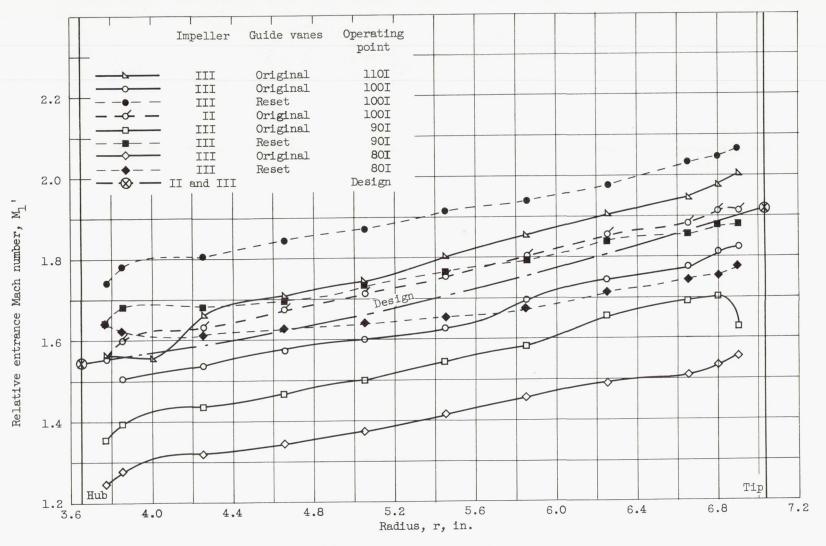
Figure 6. - Continued. Performance characteristics for 14-inch supersonic compressor rotor with supersonic leading edge.



(c) Equivalent stagnation enthalpy rise.

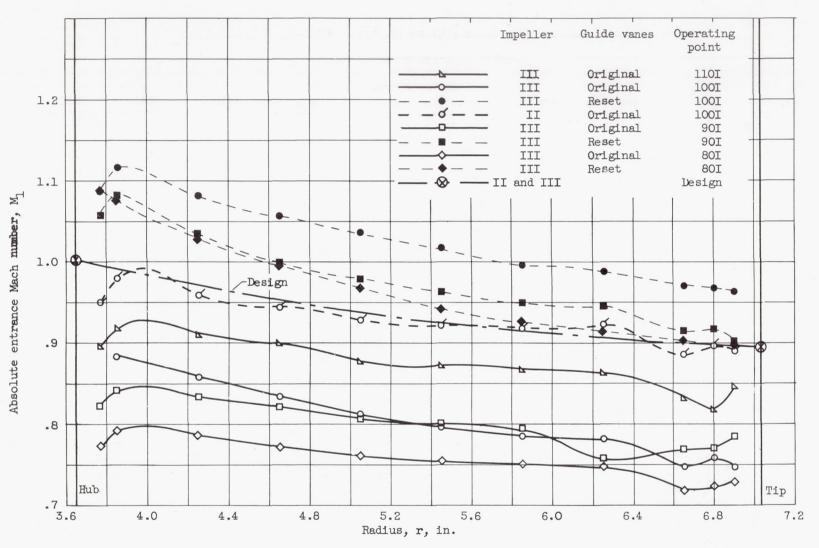
Figure 6. - Concluded. Performance characteristics for 14-inch supersonic compressor rotor with supersonic leading edge.





(a) Relative entrance Mach number.

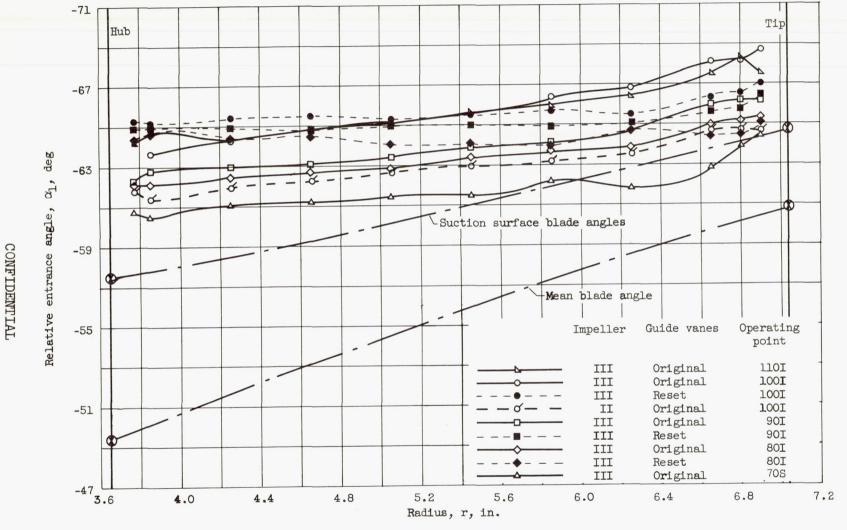
Figure 7. - Conditions at station 1 for various speeds.



(b) Absolute entrance Mach number.

Figure 7. - Continued. Conditions at station 1 for various speeds.





(c) Relative entrance angle.

Figure 7. - Continued. Conditions at station 1 for various speeds.



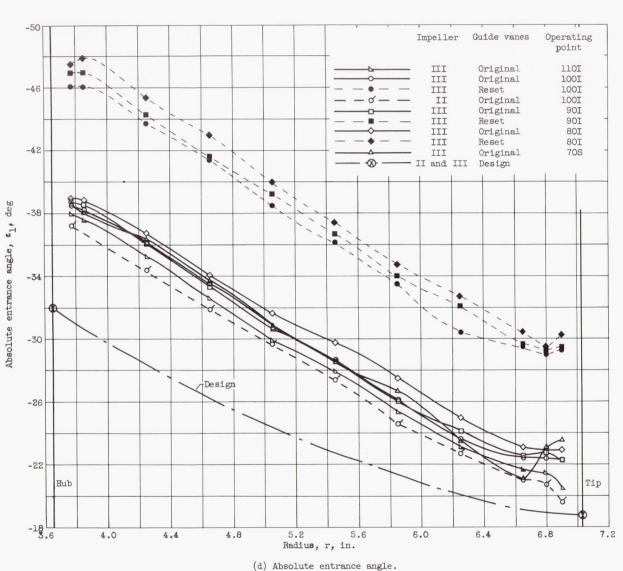


Figure 7. - Concluded. Conditions at station 1 for various speeds.

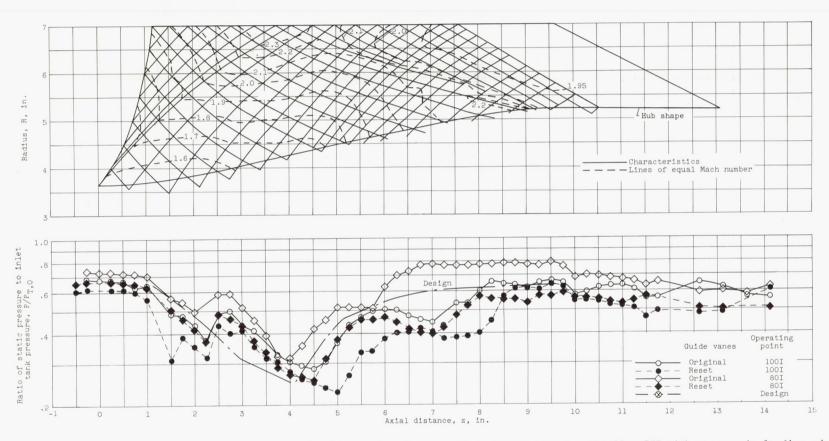


Figure 8. - Static-pressure distribution along impeller casing for several operating points. Impeller III with supersonic leading edge.

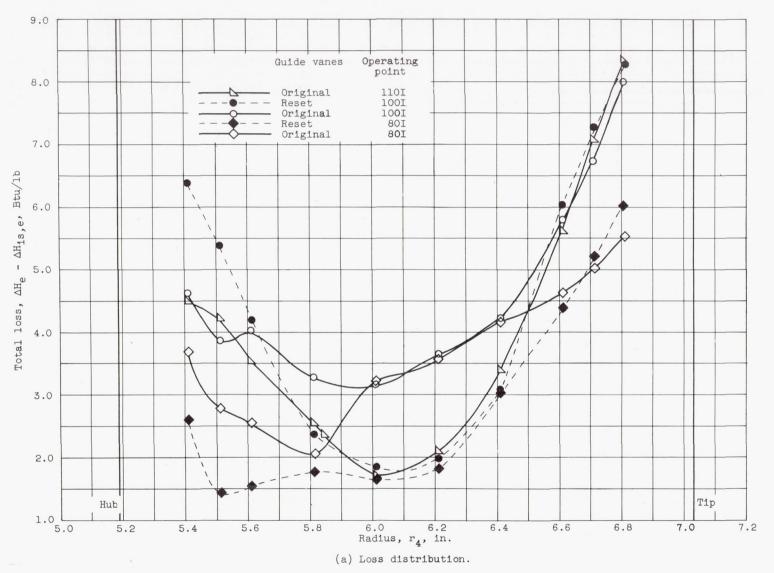
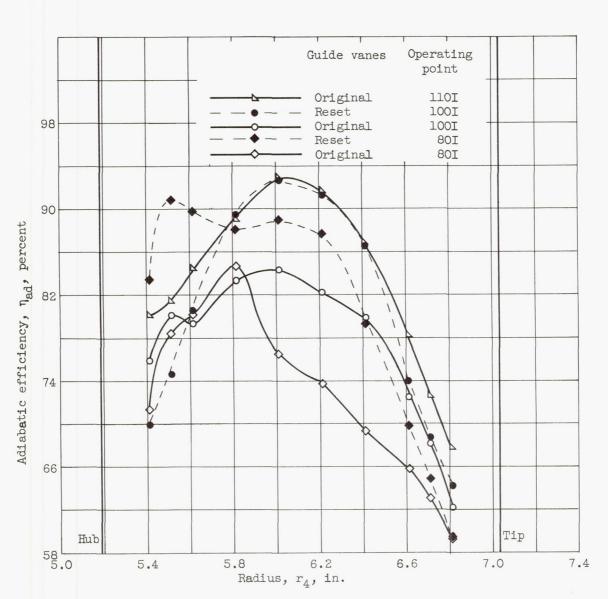
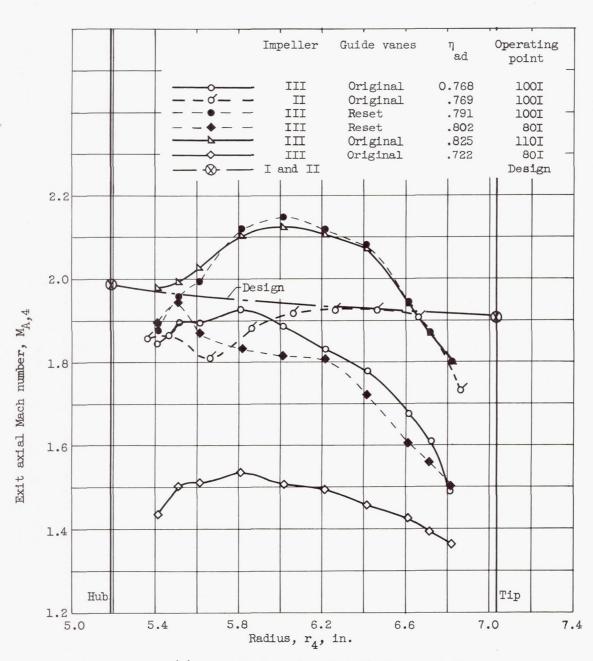


Figure 9. - Conditions at station 4 for various speeds.



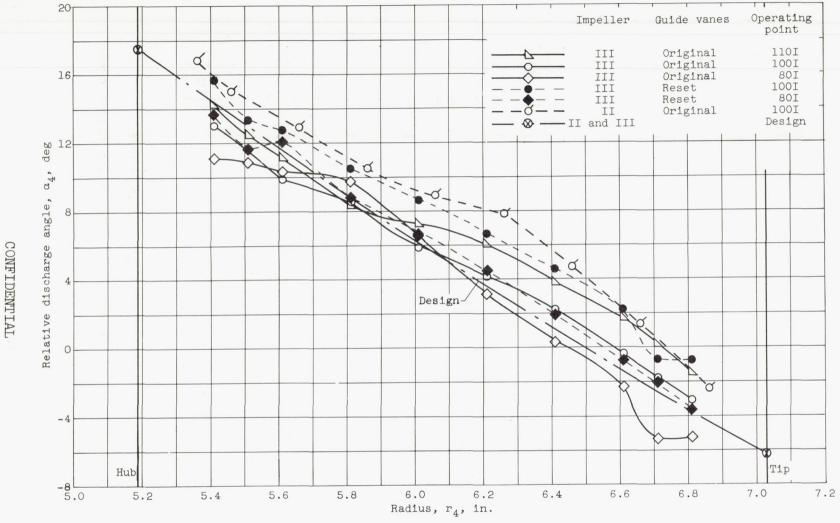
(b) Adiabatic efficiency distribution.

Figure 9. - Continued. Conditions at station 4 for various speeds.



(c) Axial Mach number distribution at exit.

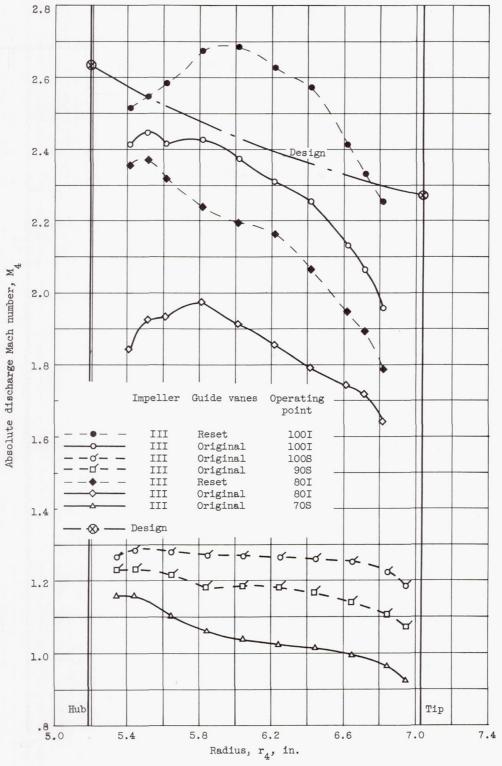
Figure 9. - Continued. Conditions at station 4 for various speeds.



(d) Relative discharge angle distribution.

Figure 9. - Continued. Conditions at station 4 for various speeds.

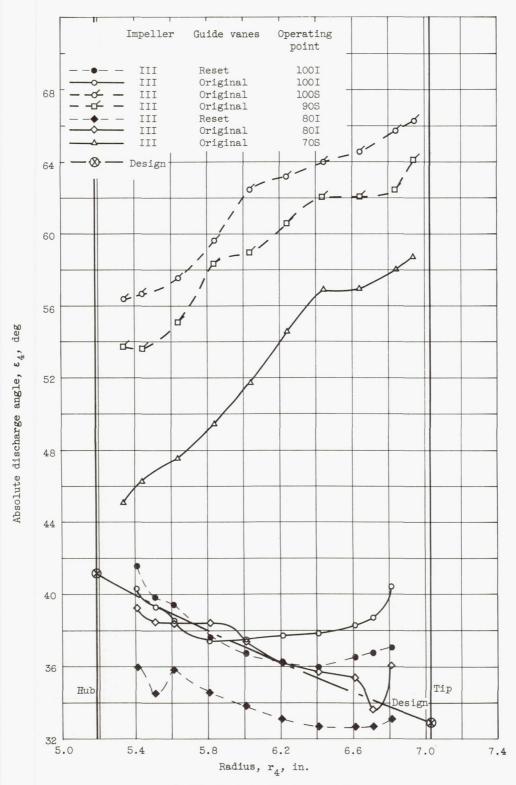




(e) Absolute discharge Mach number.

Figure 9. - Continued. Conditions at station 4 for various speeds.





(f) Absolute discharge angle.

Figure 9. - Concluded. Conditions at station 4 for various speeds.

